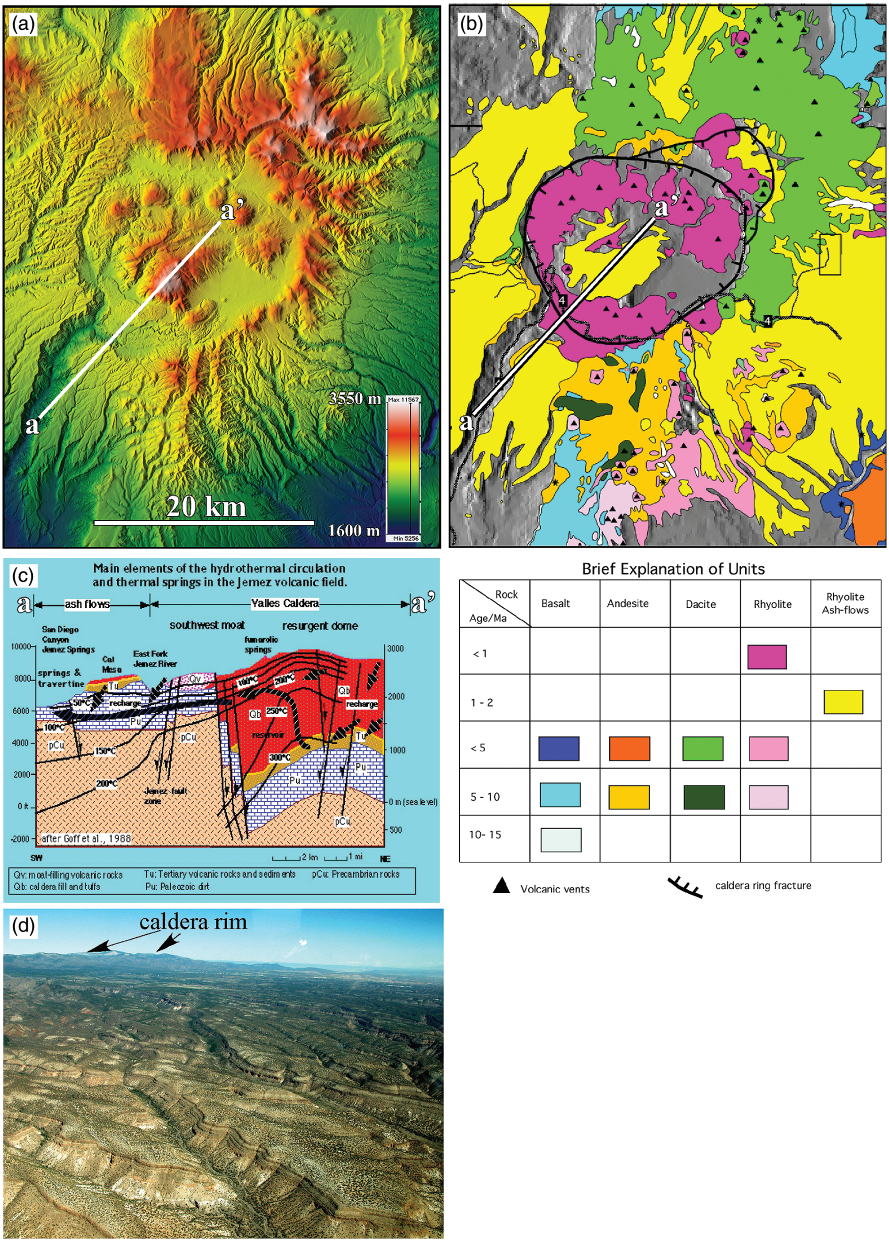

Figure 4.5. (a) Digital shaded relief map of the Valles Calderas, near Los Alamos, New Mexico. (b) Generalized geologic map of the Valles Caldera. After Luedke and Smith (1978) and Smith *et al*. (1970). (c) Schematic section (after Goff *et al*., 1989) from the caldera center through the south margin and down the prominent valley on the southwest flank illustrating the principal characteristics of hydrothermal circulation and relationship to down-gradient springs and spring deposits. Similar circulation patterns may have existed shortly after formation of the highland paterae type calderas on Mars (see, for example, Figure 4.4a). (d) Oblique air photo of valleys cut into the extensive layered sheets of Bandelier ash flow tuffs that were erupted during caldera formation; view west from vicinity of the Rio Grande; note distance from the caldera rim.

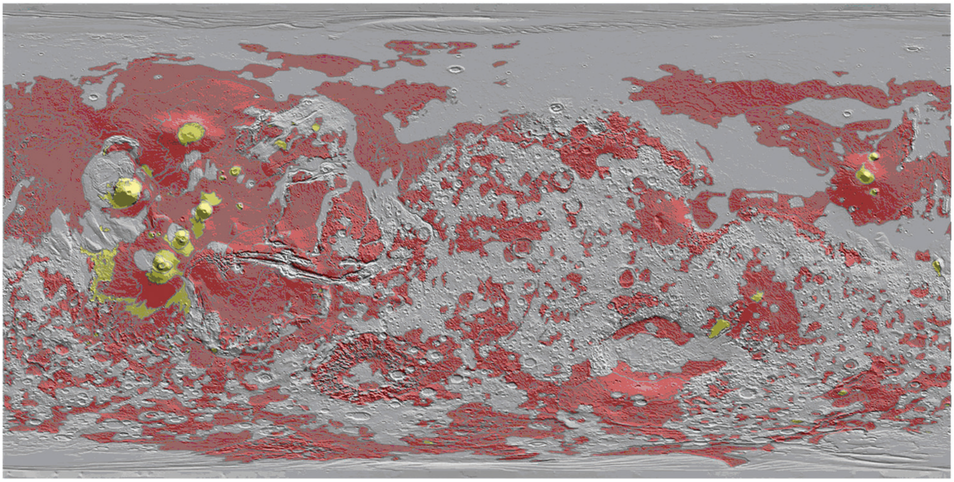

Figure 5.1. Distribution of possible flood lavas on the surface of Mars. Simplified from global maps (Scott and Carr, 1978; Scott and Tanaka, 1986; Tanaka and Scott, 1987; Greeley and Guest, 1987) and placed over MOLA global shaded relief topographic map. Areas in red have been either mapped as flood lavas or as likely to contain modified flood lavas. Yellow shows other primarily volcanic units. All remaining materials are shown in light blue. The red areas cover 47% of the surface of Mars, which is marginally

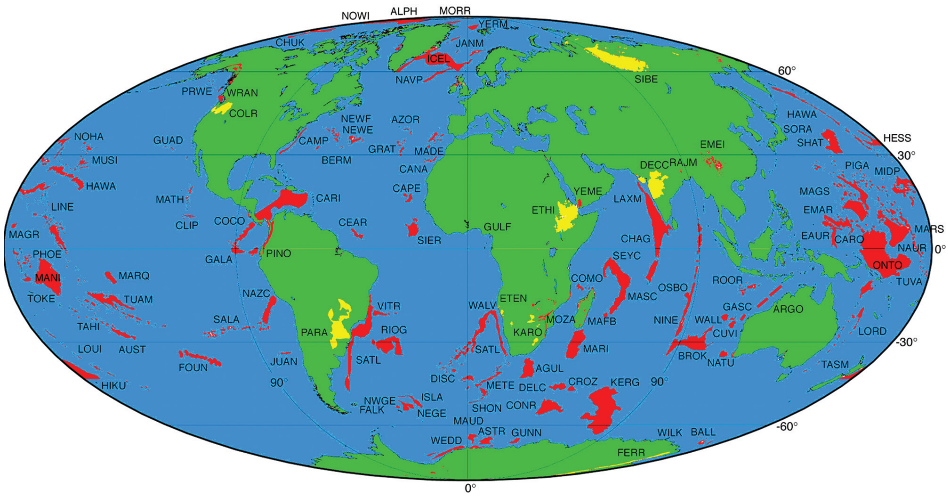

Figure 5.5. Map of Recent ($\leq$250 Ma) Large Igneous Provinces (LIPs) on Earth. Well-preserved continental flood basalt provinces listed in Table 5.2 are depicted in yellow, other LIPs in red. While recent LIPs only cover a few percent of Earth's surface, it is important to note that this only represents a few percent of Earth's geologic history. Map after Coffin and Eldholm (1994). Abbreviated names listed in full in Coffin and Eldholm (1994).

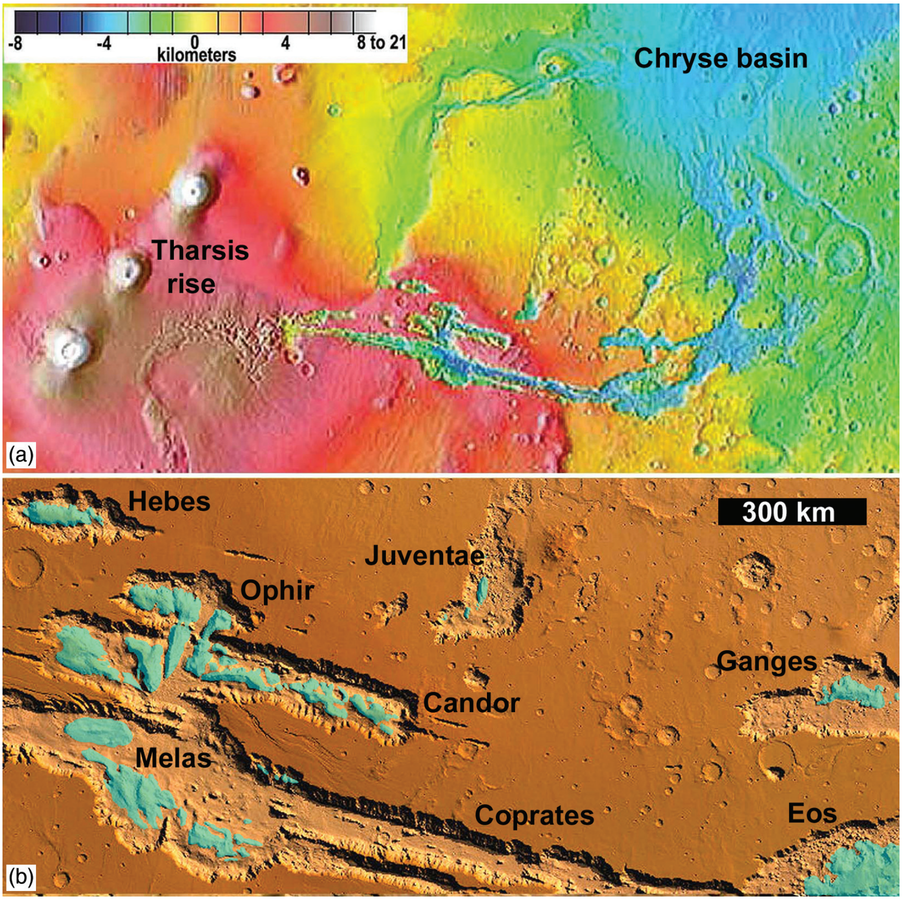

Figure 7.1. The 3000 km long canyon of Valles Marineris, Mars. (a) MOLA (Mars Observer Laser Altimeter) topographic view showing volcanoes of the Tharsis rise, on the west, Valles Marineris canyons (center) and large-scale catastrophic flood channels that drain into Chryse basin from Valles Marineris, on the east. (b) MOLA-derived three-dimensional enlarged view of central and east Valles Marineris showing interior layered deposits in blue. Note topographic lows in central Melas and Juventae Chasma, and high partial wall separating Candor Chasma from Melas Chasma.

Figure 9.4. Oblique view of a star dune in the Ibex Dunes, California. The star dune is ~30 m tall. The dark patches at the base of the dune consist of dark pebbles and granules derived from the nearby mountains, some of which have accumulated into large ripples of 2 to 8 m wavelength, over a sand substrate, possibly analogous to some ripple-like features on Mars (see Figure 9.8). JRZ, 2/03.

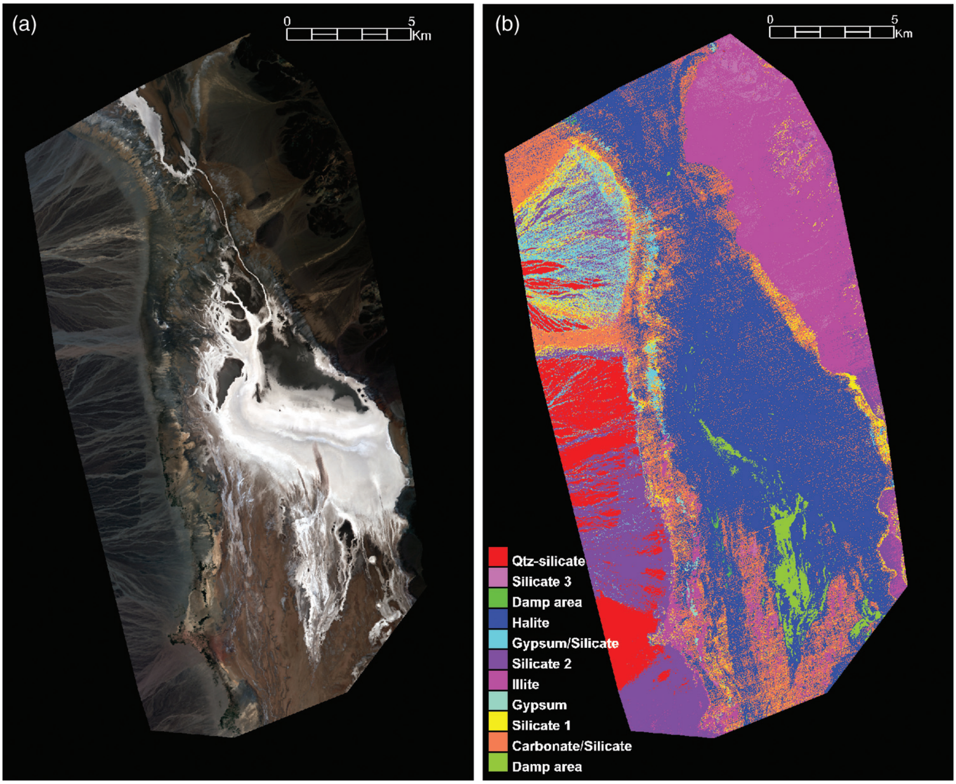

Figure 13.12. MASTER views of Badwater Basin, Death Valley, California. (a) Approximate true color image created using the MASTER 0.654, 0.542, and 0.460 µm reflectance bands. (b) Spectral classification map of MASTER thermal infrared bands.

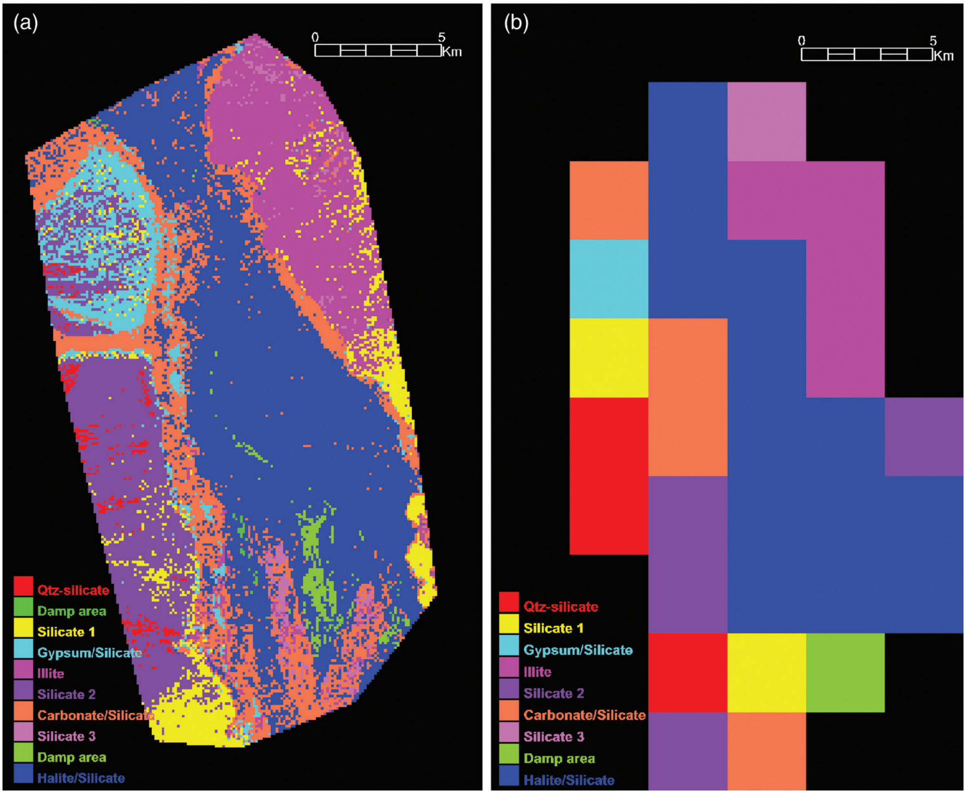

Figure 13.13. The effects of spatial resolution on spectral classification mapping of Badwater Basin. (a) MASTER thermal infrared emissivity data were degraded to the 100 m/pixel spatial resolution of the THEMIS instrument and then spectrally classified as in Figure 13.12b. (b) The same data were degraded to 3 km spatial resolution (approximately equal to TES resolution) and then spectrally classified. Spectral endmembers used to classify the TES-resolution data were taken from THEMIS-resolution data because there were insufficient pixels available at TES resolution to provide useful endmembers. Note that the typical spatial/spectral evaporite patterns on the western margin of the basin are clearly visible at THEMIS resolution, but are lost at TES resolution.

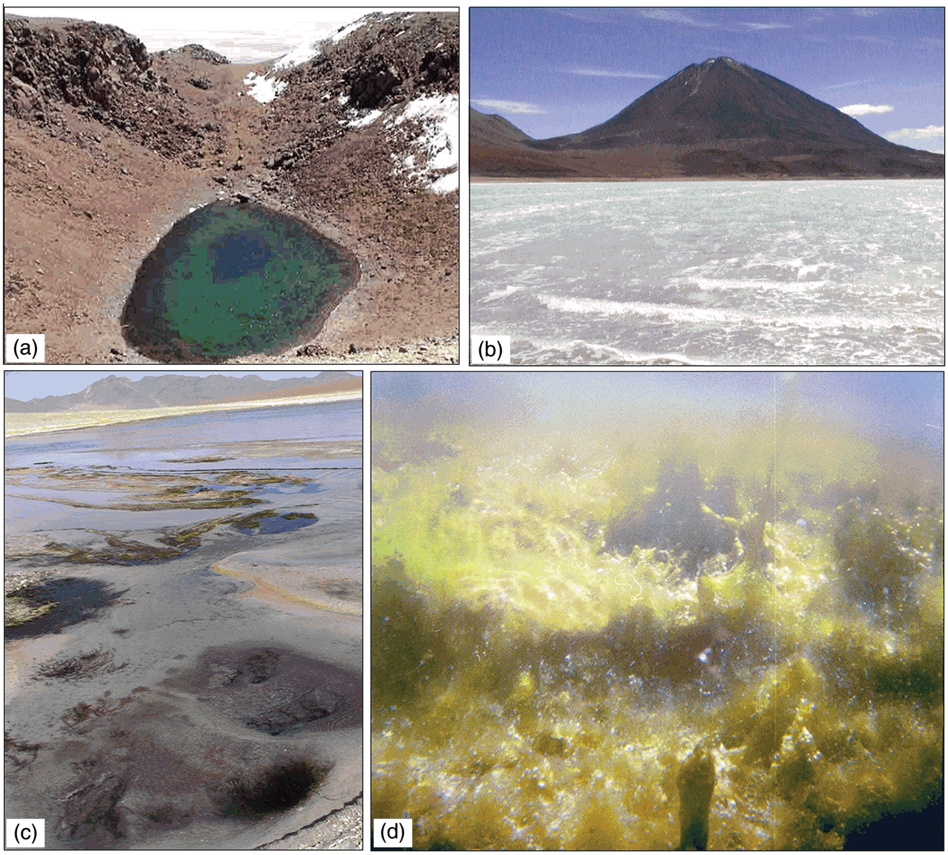

Figure 14.2. (a) Licancabur lake 100 m below the summit rim. Paleoshorelines are visible. The lake currently ~100×90 m and possibly up to 10 m deep, may have reached 65 m and ~200 m in diameter at its peak. (b) Laguna Verde with Licancabur in the background. (c) Hydrothermal springs in Laguna Blanca and algal mat. (d) Oxygen producing algae in the "Thermales" hot spring. Algae abound in the +36 °C water. Credit photographs: Brian H. Grigsby and Nathalie A. Cabrol.

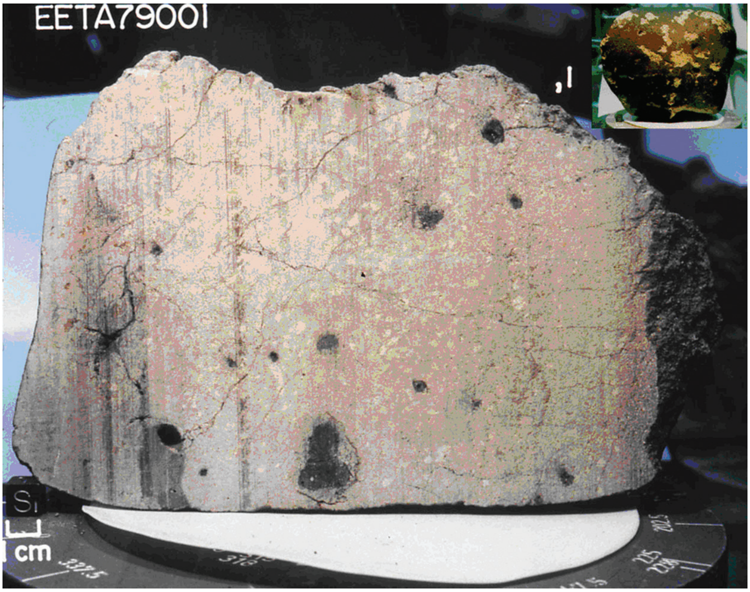

Figure 16.1. The Martian meteorite EETA 79001 was found in Elephant Moraine, Antarctica in 1979. This meteorite is a basaltic rock of the Shergottite class of Martian meteorites. The inset shows the original sample with its fusion crust, while the larger image shows a sawn face and the igneous texture. The dark areas on the cut face are impact melt pockets that contain trapped Martian atmosphere whose composition is the strongest evidence for a Martian origin for this meteorite.

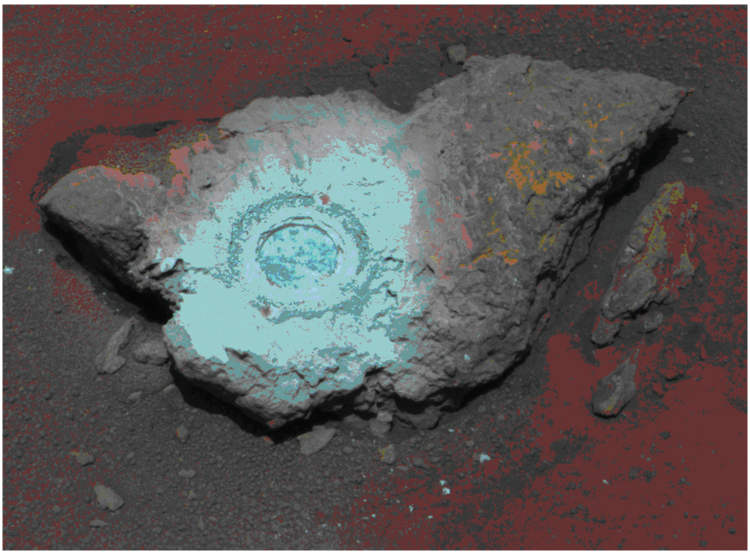

Figure 16.2. The Mars Exploration Rover Opportunity studied a rock dubbed 'Bounce' as shown in this false-color composite taken on sol 68. The 40 cm long rock was drilled to a depth of 7 mm by the rover's rock abrasion tool. The chemical composition of this sample measured by the Rover's Alpha Particle X-ray Spectrometer is nearly identical to the Martian meteorite EETA 79001 illustrated in Figure 16.1.